JOURNAL OF RENEWABLE ENERGY AND SMART GRID TECHNOLOGY

Vol. 21, No. 1, January-June 2026

Optimized Power Quality in Grid Systems Using PV-Based UPFC and Advanced ANN Control Approach

Gadupudi Lakshminarayana[1*], Sreedevi Saravanakumar[2], Malapati Venkateswarlu[3], Thankaraj Retna Bai Premila[4]

[1]Department of Electrical and Electronics Engineering, VNR Vignana Jyothi Institute of Engineering and Technology, Telangana 500090, India

[2]Department of Electrical and Electronics Engineering, Sriram Engineering College, Tamil Nadu 602024, India

[3]Department of Electrical and Electronics Engineering, Dr Samuel George Institute of Engineering and Technology, Andhra Pradesh 523316, India

[4]Department of Electrical and Electronics Engineering, Vels Institute of Science, Technology & Advanced Studies, Tamil Nadu 600117, India

***Corresponding author's email:** lakshminarayana_g@vnrvjiet.in

Article info:

Received: 17 April 2025
Revised: 11 November 2025
Accepted: 24 November 2025
DOI:
10.69650/rast.2026.261699

Keywords:

Power Quality (PQ)
UPFC
ANN Controller
Single Switch Boost-Cuk
Pelican Optimized RNN

ABSTRACT

Nowadays, grid power losses and Power Quality (PQ) issues are inducing various problems in power systems, which need to be addressed and rectified for attaining enhanced and smooth functioning. These PQ issues are generated as a result of differing values between generated and load power, which further produces fluctuations within the power supply. Hence, to overcome these limitations, an innovative control approach is proposed for attaining optimum power flow by using a Unified Power Flow Controller (UPFC). The proposed UPFC is combined with an Artificial Neural Network (ANN) controller for improving the performance efficiency of the UPFC. The ANN controller-aided UPFC rectifies the PQ issues, including sag and swell. Additionally, to provide a consistent and unlimited power supply to the DC link, a photovoltaic (PV) system is incorporated with a single-switch boost-Cuk (SSBC) converter for boosting the PV power generation process. For attaining maximum power extraction and tracking maximum power, a new Pelican Optimized Recurrent Neural Network (RNN)-based Maximum Power Point Tracking (MPPT) technique is utilized. Furthermore, to validate the proposed model, MATLAB/Simulink is utilized and the obtained results depict improved PQ with reduced losses. Therefore, the overall system attains improved power quality, thereby, enhancing the power system functioning.

1. Introduction

The need for PQ has become more essential as they affect the power generation process [1]. The distributed energy generation system is capable of providing electricity to various loads, including traditional grids, micro-grids and smart grids, however, unpredictable variations in load or power supply leads to increased fluctuations, voltage instability and reduced reliability [2-3]. Due to this reason, power electronic devices are incorporated which in turns produce a great impact on the power causing PQ like voltage swell and sag, reduced power factor and fluctuations in the output voltage [4-5]. To prevail over these issues various approaches are innovated Table.1, such as optimum power quality enhancement [6], unified power quality conditioner[7] and Distributed Power Factor Controller (DPFC) [8] focus on improving the PQ by resolving issues associated with voltage sag and swell, thereby enhancing the voltage stability with improved reliability. Despite this, the above-stated approaches also struggle with increased complexity, implementation cost and reduced efficiency [9].

Table 1 Various PQ enhancement approaches.

Technique	Capabilities	Efficiency
STATCOM [10-11]	Reactive Power Control	Moderate
UPQC [8]	PQ Improvement	Moderate
DVR [12]	Swell/Sag rectification	Low

Thus, UPFC methods are widely considered as they provide optimum power flow control by simultaneously managing both active and reactive power, thus increasing the grid stability and power flow [13]. To further improve the UPFC efficiency, various optimized control practices are introduced such as in [14], where the author developed a UPQC using Optimized Fractional Order Proportional Integral Derivatives (O-FOPID) controller for enhancing the performance of UPQC. The integration of O-FOPID provides improved UPQC operation by improving it performance in terms of stability and robustness under varying conditions.

However, this approach also faces certain challenges including parameter sensitivity which affects their consistent performance. Significantly in [15] introduced UPFC controlled using Proportional Integral Derivative (PID) for attaining enhanced power flow with increased system stability, despite this, PID controller cannot obtain the desired effective performance as it struggles with nonlinear loads, parameter variations and other interferences in power system.

The PSO-based controller has improved voltage regulation, harmonic suppression, and reactive power compensation. PSO algorithm is computationally intensive, especially when dealing with large-scale systems [16]. Then, the GA based controller enhancing power quality performance. GA has the premature convergence or getting trapped in local optima [17]. In [18] the authors developed a Fuzzy

Logic based UPQC system for increasing the PQ by efficiently reducing the harmonics, voltage swell and sag within the system, nevertheless, FLC based control produces increased computational complexity.

In addition to this, the required power for the DC-link is supplied by the energy efficient PV system. The integration of PV into UPFC enables the production of clean and sustainable energy thereby, managing the load energy requirement issues [19]. To augment the PV power production, DC-DC converters play a major role, various conventional converters are existing such as [20] KSK Converter, [21] 7-Level Voltage Source Converter (VSC) and [22] Cuk Converter, which possess the ability to regulate the output voltage, ensuring consistent PV power supply with enhanced energy conversion process. But these converters suffer from increased losses, reduced voltage gain, making them less applicable.

Hence, a SSBC converter is utilized which allows for increased output voltage levels by combining the benefits of both boost and Cuk converter. Consecutively, to further extract maximum power and to measure accurate MPP, MPPT technique are widely utilized, these MPPT approaches are further optimized using various optimization algorithms to improve their performance efficacy. Existing MPPT algorithms like Particle Swarm Optimization [23], Artificial Bee Colony (ABC) [24] and Perturb and Observe (P&O) [25] techniques provide accurate tracking of MPP with reduced tracking time, even though these algorithms are not widely considered as they are computationally intensive, complex and struggles with maintaining the optimal performance under constantly changing system parameters. Thus, Pelican Optimized RNN based MPPT approach(tracking efficiency of 99.8%) is deployed which outdraws the above mentioned algorithms in terms of attaining precise and accurate MPP tracking with fast tacking ability under varying environmental circumstances.

Contribution

The proposed framework incorporating an ANN-governed UPFC and a Single Switch Boost-Cuk regulated PV system integrated with a Pelican-optimized RNN-based MPPT controller, delivers significant power quality improvements. It effectively mitigates voltage sag and swell phenomena across dynamic grid conditions, thereby advancing the robustness and adaptability of PV-based UPFC systems. The following are the main contributions,

- To effectively rectify PQ issues within the power system using UPFC which performs optimum power flow control, mitigating the PQ issues such as sag and swell.
- To further attain enhanced UPFC control, ANN is implemented which depicts enhanced control performance.
- To provide sustainable and consistent energy supply to the DC link, PV system is incorporated with SSBC converter for regulating the PV output voltage.
- To attain increased PV power generation with accurate tracking of MPP, Pelican Optimized RNN based MPPT is deployed which achieves precise MPP tracking with rapid tracking time.

2. Proposed Modelling

Fig. 1 illustrates the proposed system block diagram integrating RES to achieve regulated voltage and load management using advanced control approaches. Initially, PV system generates energy the DC link, but the initial output from PV is quite low, thus a SSBC converter is connected. The implementation of the SSBC converter boost and step-up the PV production, thereby providing regulated power supply. In addition to this, POA-RNN based MPPT improves the PV generation by enabling maximum power extraction and helps with accurate and precise tracking.

UPFC consisting of a series converter and a shunt converter is connected to the power system, where series converter handles the voltage and power while, shunt converter regulates the reactive and active power within the system by regulating voltage and reactive power consumption. Later, the LC filter further removes and smoothens the high frequency harmonics. Lastly, the ANN controller utilized regulates the UPFC performance and the PWM generator provides the required switching pulses for the both the series and shunt converters thereby, assuring sustainable and effective system performance. Therefore, the overall proposed system acquires improved and enhanced management of PQ issues within the grid based power system.

2.1 Modelling of UPFC

UPFC which is mostly utilized power regulation in a transmission line. Fig. 2 represents the architecture of UPFC and the power generated by shunt active power filter S_f and series active power filter S_C is given by equations (1) and (2),

$$S_C = P_C + j\swarrow_C \quad (1)$$

$$S_f = V_C I_f \quad (2)$$

$$I_S V_C \cos\phi\ (s) = P_C \quad (3)$$

$$I_{sV_C} \sin\phi(s) = \swarrow_C \quad (4)$$

Here, P_C and Q_C indicates the absorbed active and reactive power, V_C refers to the load voltage, ϕ indicates the tardy power factor and I_f denotes the divergence between the input and the load current.

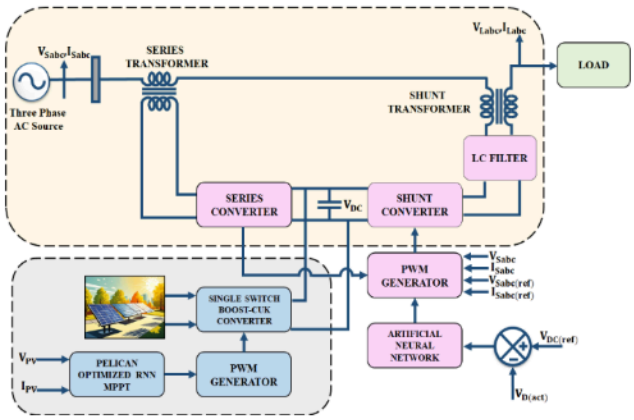

Fig. 1 Proposed System Block Diagram.

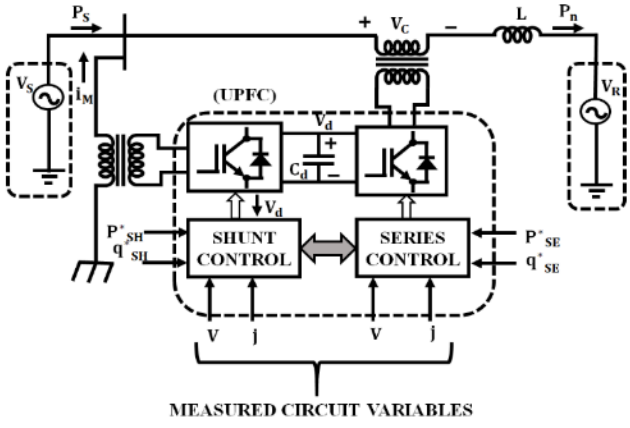

Fig. 2 UPFC Structure.

A UPFC is utilized to control and optimizing the power flow in high voltage power systems. UPFC controls the power flow by regulating the signal's phase angle and voltage magnitude, for which a series and shunt connected power converters play a major part. The series connected converter is deployed to control the voltage on the transmission line by removing voltage from the line, while the shunt connected converter is connected in parallel with the transmission line is deployed to control the reactive power. UPFC is an effective and advanced tool for increasing the performance efficiency of the power system. However, to assure controlled and effective UPFC performance controller plays a major role, thus an ANN controller is deployed to attain effective UPFC control.

2.2 Modelling of ANN Controller

ANN is generally structured based on the neural structure of the brain, which replicates its functioning behaviour. ANN is an innovate commuting by producing large number of parallel network to rectify particular issues as depicted in Fig. 3. The working process of ANN is exhibited in simpler patterns to attain high computational rate because of larger parallelism with increased fault tolerance ability. The training process is carried out using the back propagation algorithm, where weights and thresholds are initialized randomly and updated iteratively.

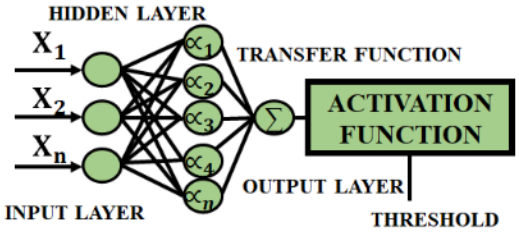

Fig. 3 ANN controller for Shunt Converter.

a) Initialization: The first step is to initialize, weights and threshold levels are randomly allocated in small region.

b) Activation: The activation functions process hidden neuron outputs, while the error gradient at both the hidden and output layers helps refine the weights. In this step, the output attained from the neurons in the hidden layer are evaluated.

$$sigmoid\left[\sum_{i=1}^{n} w_{ij}(p).x_i(p) - \theta_i\right] = Y_j(p) \quad (5)$$

Where, n is number of input neurons $j$and output of outer layer is given as,

$$sigmoid\left[\sum_{i=1}^{m} w_{ik}(p).x\,jk(p) - \theta_k\right] = Y_k(p) \quad (6)$$

c) Training: The training data consists of system operating conditions such as load voltage, reactive power variations, and power quality disturbances including sag and swell. In this step, the error gradient for neurons in the outer layer is determined using,

$$\delta_k(p) = [1 - y_k(p)]_{y_k}(p).e_k(p), \epsilon_k(p) = y_{dk}(p) - y_k(p) \quad (7)$$

Rectified weight is depicted as,

$$\Delta w_{jk}(p) + w_{jk}(p) = \Delta w_{jk}(p+1) \quad (8)$$

The updated weights at the output layers is given as,

$$w_{jk}(p) + \Delta w_{jk}(p) = \Delta w_{jk}(p+1) \quad (9)$$

The hidden layer's error gradient us determined using,

$$[1 - y_j(p)]y_j(p)\sum_{k=1}^{1} w_{jk}(p)\delta_k(p) = \delta_j(p) \quad (10)$$

The corrected weights are evaluated as,

$$\delta_j(p)\alpha x_i(p) = \Delta w_{jk}(p) \quad (11)$$

And the upgraded weight at the hidden layer is,

$$w_{jk}(p+1) = w_{jk}(p) + \Delta w_{jk}(p) \quad (12)$$

d) Iteration: The fourth step is to increase the p by 1 stage and the procedure is continued until the chosen error criterion is fulfilled.

The data used to train the ANN in the DC-link voltage controller was obtained from MATLAB/Simulink simulations of the proposed hybrid system. Solar irradiance, wind speed, DC-link voltage, and load current are all input features, with the reference DC-link voltage (400 V) being the goal output. The network was trained via the Levenberg-Marquardt method, With Mean-Squared Error (MSE) as the cost function. The error is defined as,

$$e(t) = V_{DC,ref} - V_{DC,act} \quad (13)$$

The ANN reduces this inaccuracy to deliver voltage stability. The grid, source and load are assumed to be balanced in the development of the model and disturbances are primarily restricted to swell and sag conditions. The PV system is thought to function with consistent temperature and irradiance, providing a constant input for the converter.

2.3 Modelling of PV system

The circuit of the PV system is illustrated in Fig. 4 consists of diode which is coupled in shunt to the load and making the produced current proportional to light intensity. PV system output power is calculated using,

$$P = V \times I \quad (14)$$

Here, P represents Power, V indicates voltage and I implies current. Significantly, the current on output side is produced by PV is given by,

$$I_{pv} = I_{ph} - I_0\left[exp\left(\frac{V + IR_s}{V_T}\right) - 1\right] - \frac{V + IR_s}{R_{sh}} \quad (15)$$

Where, I_{ph} refers to photo-current and I_0 refers to diode reverse saturation current, R_s and R_{sh} denotes the series and shunt resistance and V_T implies the thermal voltage.

V_T is evaluated using,

$$V_T = \frac{\alpha N_s kT}{q} \quad (16)$$

Where, α indicates the diode ideal factor, N_s denotes to the number of series linked cells and q refers to the electron charge. Further to boost the PV power production converter is considered essential.

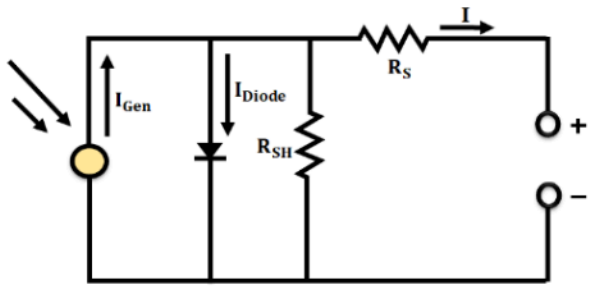

Fig. 4 Equivalent Circuit of PV system.

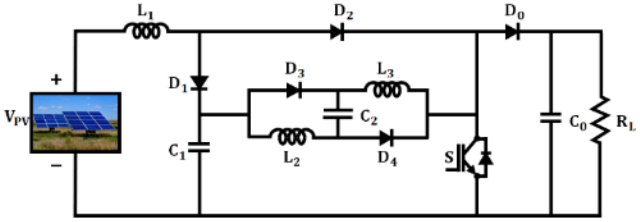

Fig. 5 Circuit Diagram of SSBC converter.

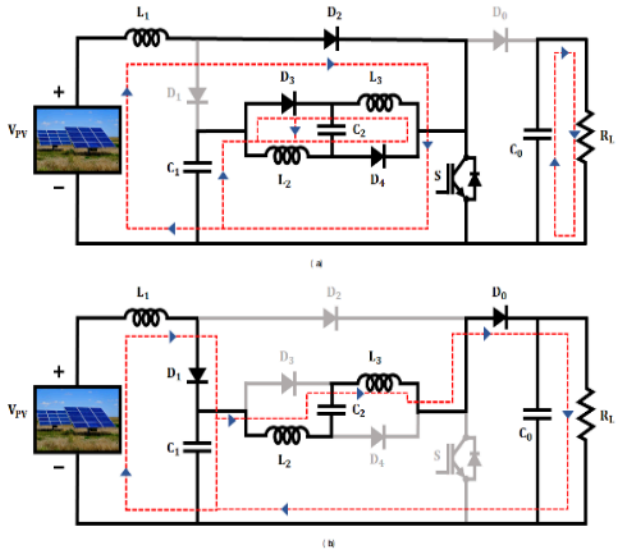

Fig. 6 Converter modes of operation.

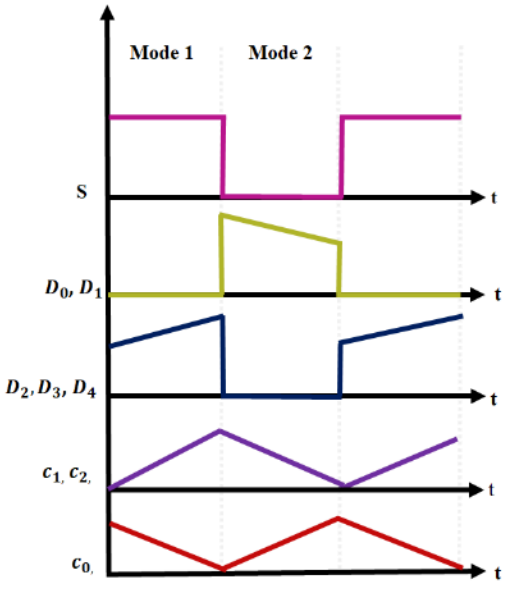

Fig. 7 Timing Waveform.

2.4 Modelling of SSBC converter

The SSBC converter is the integration of both boost and Cuk converter, thus containing the benefits of both the converters. The proposed converter circuit diagram is illustrated in Fig. 5 contains a single switch, Three inductors (L_1 , L_2 and L_3), Three capacitors (C_0, C_1 and C_2) and Five diodes (D_0, D_1, D_2, D_3 and D_4) respectively.

The proposed converter operates in two following modes which are revealed in Fig. 6 and its corresponding timing waveform is shown in Fig. 7.

Modes of Operation

i) Mode 1: Switch (ON)

Switch S is kept in ON state during this mode, where inductors L_2 and L_3 gets charged while diodes D_2, D_3 and D_4 are forward biased. Here, capacitor C_1 and C_2 charges and L_1 discharges.

ii) Mode 2: Switch (OFF)

During mode 2 switch S is turned off where inductor L_1 gets charged while diodes D_0 and D_1 are turned ON. In this mode capacitor C_0 gets charged and L_2 and L_3 discharges.

The voltage ratio is expressed using,

$$V_0 = \frac{1}{(1-D)^2} V_{in} \tag{17}$$

$$\begin{aligned} L_1 &= V_{in} - V_{d(D)} - V_{d(S)} - 2\,V_{d(L)} \\ V_C &= V_{in} - V_{d(S)} - V_{d(D)} - 2\,V_{d(L)} \\ V_L &= V_{C1} - V_{d(S)} - V_{d(L)} \end{aligned} \tag{18}$$

Where, $V_{d\,(L)}$ represents the voltage drop across inductors, similarly, $V_{d\,(D)}$ and $V_{d\,(S)}$ denotes the voltage drop across the diode and switch. The voltage drop is regarded in similar to,

$$V_{d(L)} - V_{d(S)} - V_{d(D)} = V_d \tag{19}$$

By volt second balance law for inductor L ,

$$\int_0^{DT_s} (V_{in} - 4V_d)\,dt + \int_{DT_s}^{T_s} \times \left(\frac{2V_{in} - V_{C1} - 7V_d}{2}\right) dt = 0 \tag{20}$$

$$V_{C1} = \left(\frac{2}{1-D}\right) V_{in} - \left(\frac{7+D}{7-D}\right) V_d \tag{21}$$

If internal voltage drop is not considered, then voltage conversion ratio is given by,

$$\frac{1}{(1-D)^2} V_{in} = V_0 \tag{22}$$

The steady-state equation during CCM is,

$$\left.\begin{aligned} V_{in} - 3\,V_d &= V_{L1} \\ V_{C1} - 3V_d &= V_{L3} \\ V_{C1} - 3V_d &= V_{C2} \end{aligned}\right\} ONstate \tag{23}$$

$$\left.\begin{aligned} V_{L1} &= V_{in} - V_{C1} - 2\,V_d \\ V_L &= \frac{2\,V_{C1} - V_0 - 6V_d}{2} \end{aligned}\right\} OFF\ state \tag{24}$$

Apply volt second balance law in L_1

$$\int_0^{DT_s} (V_{in} - 3V_d)\,dt + \int_{DT_s}^{T_s} \times (V_{in} - V_{C1} - 2V_d)dt = 0 \tag{25}$$

$$V_{C1} = \left(\frac{1}{1-D}\right) V_{in} - \left(\frac{2+D}{1-D}\right) V_d \tag{26}$$

Furthermore, to increase the converter performance and to extract maximum power from PV system Pelican Optimized RNN based MPPT algorithm is deployed which discussed in the later section.

2.5 Modelling of Pelican Optimized RNN MPPT

RNN based MPPT as depicted in Fig. 8 which utilizes data from previous iterations to improve the efficiency and RNN loops and possess a hidden memory state. RNN is capable of performing in sequence and previously stored set of information in a hidden state. In other way, RNN attains a part of its output as the input, thus enabling it to rectify the issues associated with sequential data of various sizes. RNN is highly applicable due to its low complexity. The output of RNN is attained using,

$$(W_h x_t + U_h h_{t-1} + b_h)\sigma_h = h_t \quad (27)$$

$$(W_y h_t + b_y)\sigma_y = y_t \quad (28)$$

Where, x_t, y_t and h_t denotes input, output and hidden layer vectors, W, U and b represents the vector and variables metrics and h and y indicate activation function which are given as,

$$\sigma_h(x) = \frac{2}{1 + e^{-2x}} - \quad (29)$$

$$\sigma_y(x) = x \quad (30)$$

In this approach, RNN selects temperature and solar irradiation as the input vectors, which is further used for training RNN and the obtained output is the reference current vector I_{mpp} which demonstrates the MPP's consistent functioning. Hence, MPPT plays a vital role in PV to assure that PV system is working at its maximum MPP, utilizing RNN provide accurate and reliable tracking process. Despite this, POA is integrated to further optimize RNN parameters for attaining improved convergence speed and increased accuracy.

The POA, which is inspired by pelican hunting behavior, utilized to optimize the RNN parameters. To balance exploration and computation, the population size is set to 30, and parameter bounds (learning rate, weights, and biases) are determined using stability ranges reported in previous MPPT experiments. The method terminated at 100 iterations or when the error reached 10^{-3}. Each pelican in the population represents a potential solution, and their placements in the search space are iteratively changed to increase the RNN's performance under different irradiation and temperature scenarios. The population component staring with least to the higher bound is randomly generated using,

$$x_{i,j} = rand(u_j - I_j) + I_j, j = 1,2,\ldots.,m, i = 1,2,\ldots,N, \quad (31)$$

Where, $x_{i,j}$ represents the $j\,th$variable value through $i\,th$ possible solution, N indicates the total population members, m denotes the problem variables, $rand$ implies the random number from [0, 1], I_j represents the $j\,th$ lower limit and u_j refers to the upper bound respectively. The pelicans are arranged according to the population matrix depicted in equation 6,

$$X = \begin{bmatrix} X_1 \\ \vdots \\ X_i \\ \vdots \\ X_N \end{bmatrix}_{N\times m} = \begin{bmatrix} x_{1,1} & \cdots & x_{1,j} & \cdots & x_{1,m} \\ \vdots & \ddots & \vdots & \ddots & \vdots \\ x_{i,1} & \cdots & x_{i,j} & \cdots & x_{i,m} \\ \vdots & \ddots & \vdots & \ddots & \vdots \\ x_{N,1} & \cdots & x_{N,j} & \cdots & x_{N,m} \end{bmatrix}_{N\times m} \quad (32)$$

Where, X indicates the pelican population matrix, X_i denotes the $i\ th$ pelican in the population. Considering POA algorithm, each pelican represents a particular member carrying a possible solution for the depicted problem, thus objective function is defined as,

$$F = \begin{bmatrix} F_1 \\ \vdots \\ F_i \\ \vdots \\ F_N \end{bmatrix}_{N\times 1} = \begin{bmatrix} F(X_1) \\ \vdots \\ F(X_i) \\ \vdots \\ F(X_N) \end{bmatrix}_{N\times 1} \quad (33)$$

The POA functions based on the hunting behavior of pelicans in two stages namely, Exploration phase and exploitation phase as illustrated in Fig. 9 and Fig. 10 demonstrates its corresponding Flow Chart.

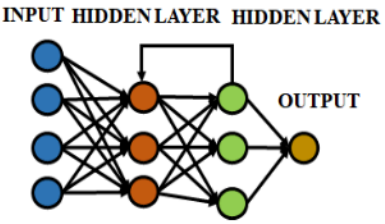

Fig. 8 RNN based MPPT.

Fig. 9 Pelican Optimization.

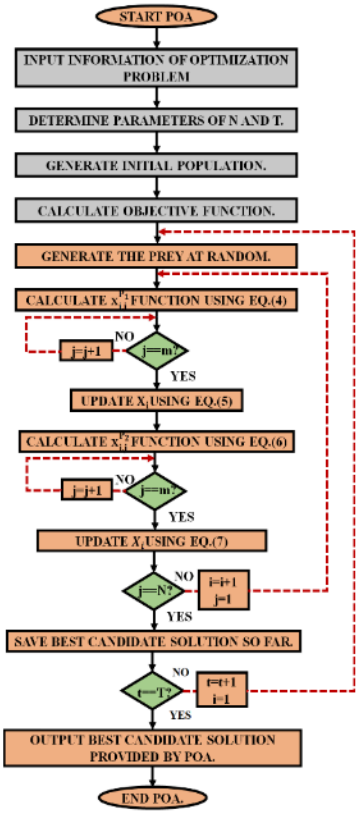

Fig. 10 POA Flow Chart.

a) Exploration phase: In this stage, pelicans look for their prey and then move towards them. This approach exhibited by pelicans is termed as the exploration and search space ability and the random selection of prey location is considered as an essential aspects of POA. This random selection allows the pelicans to adapt for exploration and navigation enabling problem solving capabilities which given by,

$$x_{i,j}^{P_i} = \begin{cases} x_{i,j} + rand\left(P_j - I\,x_{i,j}\right), & F_p < F_i; \\ x_{i,j} + rand\left(x_j - P_j\right), & else; \end{cases} \quad (34)$$

b) Exploitation phase: The Pelican lower to the water surface which illustrates their wing stretching characteristics. This determines their strategy to rise prey in that particular location, enabling them to capture more prey. Thus, inspired by this strategy of the pelicans, POA is developed to lead convergence towards the favorable region within the hunting zone. Hence, this tactic augments the POA algorithms prospective for exploiting local regions thereby, improving the ability for conducing enhanced searches, the hunting approach of pelican is given by,

$$x_{i,j}^{P_2} = x_{i,j} + R.\left(1 - \frac{t}{T}\right).(2rand - 1).x_{i,j} \quad (35)$$

Here, $x_{i,j}^{P_2}$ denotes the ith pelicans new position in the $j\ th$ dimension, R indicates the nearby radius immediate population members. The $1 - \frac{t}{T}$ is considered essential as they adjust the search location for each pelican thus, making POA perform more effectively by the optimum exploration of the search space. The random prey choosing and adaptive radius tuning further enhance its strong global and local search abilities. Therefore, the system as a whole ensures improved PQ management.

Integration of POA-RNN with BPTT training

A RNN that processes sequential data using internal feedback loops, allowing it to recall previous information and capture time-dependent patterns. RNN parameters (weights and biases) are typically updated using Back propagation Through Time (BPTT), which lowers prediction error using gradient-based optimization. In this work, the POA is utilized to enhance before beginning gradient training. The POA is used to conduct a global search for near-optimal initial weights, biases, and learning-rate values for the RNN. This initialization phase allows the network to avoid poor local minima and improves convergence. After POA selects the best candidate parameters, the RNN is fine-tuned using the BPTT technique to locally minimize the loss function. During POA optimization, the Mean-Squared Error (MSE) between predicted and actual MPPT reference power is employed.

$$F(W, b, \alpha) = \frac{1}{N}\sum_{i=1}^{N}\left(P_{pred}(i) - P_{ref}(i)\right)^2 \quad (36)$$

Here, $W, and\ b$ are RNN weights and biases, while , α is the learning rate. This hybrid POA-BPTT system efficiently blends metaheuristic search exploration with gradient-based learning precision. Fig. 11 depicts the overall training flow, demonstrating the convergence improvement gained by initializing the RNN with POA before BPTT fine-tuning. This hybrid POA-BPTT framework utilizes benefit of POA's global search capability and BPTT's quick convergence, resulting in higher accuracy and shorter training times than traditional training.

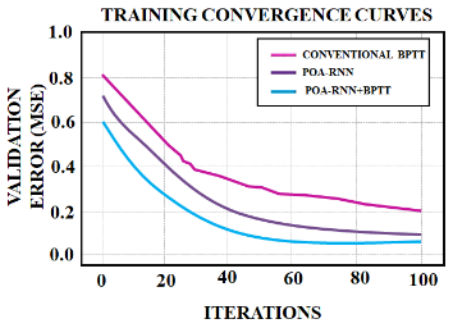

Fig.11 Training convergence comparison of RNN configurations.

Convergence curves for RNN training in three configurations: conventional BPTT, hybrid POA-initialized RNN with BPTT, and POA-only. The suggested hybrid model achieves the minimum validation MSE in 60 iterations, whereas the typical BPTT requires approximately 110 iterations. This demonstrates that POA initialization successfully steers the RNN toward faster and more stable convergence.

3. Results And Discussion

Develoed system is appliedin MATLAB/Simulink toevaluate its performance characteristics in terms of control, tracking and PQ improvement. The obtained outcomes are discussed and assessedby analysis, which is elaborated and detailed in the below section along with its parameter specification listed in Table 2.

Table 2 Parameter Specification.

Parameters	Values
PV System	
Number of cells in parallel connection	16
Short Circuit current	$8.95A$
Number of cells in series connection	2
Open Circuit voltage	$37.25V$
SSBC converter	
Switching Frequency	$10kHz$
$\boldsymbol{L_1, L_2, L_3}$	$4.7mH$
$\boldsymbol{C_1}$	$22\mu F$
UPFC	
Turns ratio	1:1
Resistence	0.28Ω
Leakage Inductance	$0.3mH$
V_{dc}	$600V$
C_{dc}	$4700\mu F$

PV System and Converter Output Waveforms

Fig. 12(a) and (b) represents the PV temperature and intensity waveform, where both the temperature and intensity is maintained at constant value throughout the depicted time duration of 0.8 seconds. The PV temperature is fixed at 35°C and the intensity is fixed at 1000 W/Sq-m respectively, indicating smooth and consistent temperature and intensity with zero fluctuations.

Fig. 13(a), (b), (c) and (d) indicates converter input and output voltage and current waveform, first graph containing the input voltage of the converter shows that, input is constantly maintained at 74V through entire time period with null fluctuations. While, the second graph shows that, input current is rapidly raised to around 2400 A and further maintained at that specific current. Meanwhile, the third and fourth graph displays voltage and current on output side of SSBC converter, output voltage initially begins with zero and further drops down beyond -1000 V and settles down after 0.6 seconds with irregular fluctuations. The output current settles down after 0.2 seconds and later remain fixed during the depicted time duration.

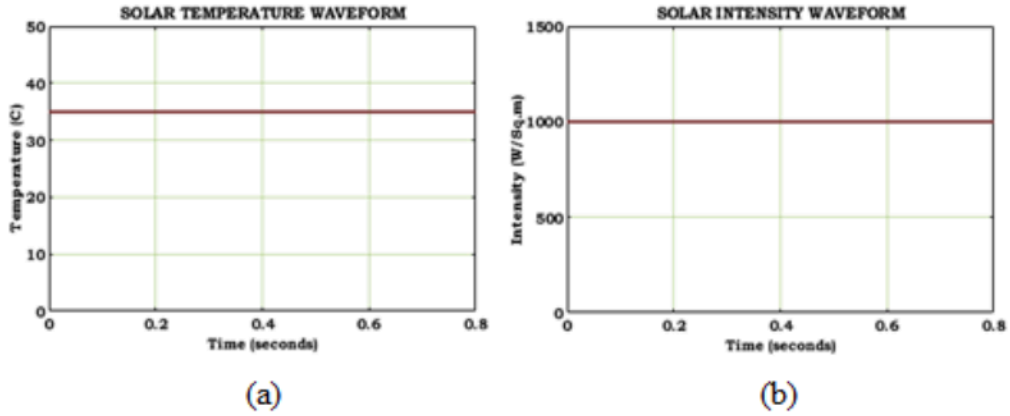

Fig. 12(a) PV Temperature (b) Intensity.

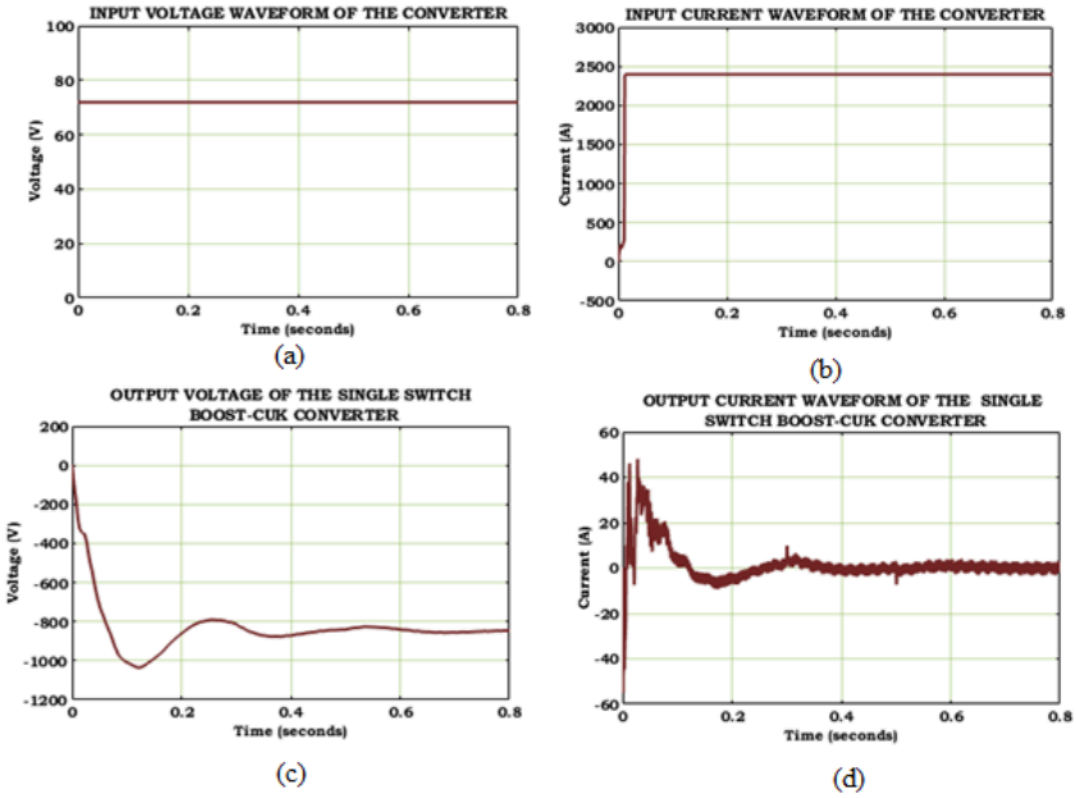

Fig. 13 Converter 's input (a) voltage (b) current and (c) voltage (d) current on output side.

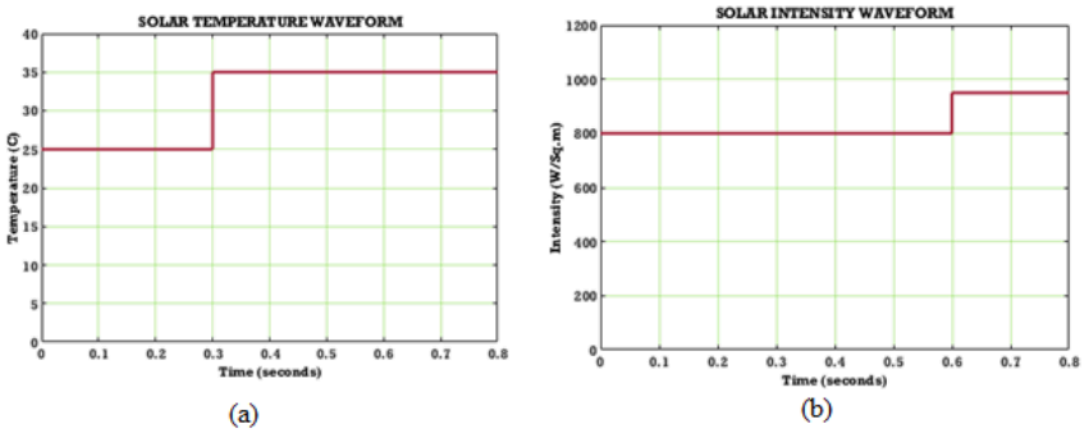

Fig. 14(a) PV Temperature (b) Intensity in varying condition.

The temperature and intensity is presented in Fig. 14(a) and (b). The temperature is varied in the beginning and settled at 35 °C and intensity is sustained at 950 (W/sq.m) in the entire system.

The input voltage is altered and maintained at 80V and input current is randomly varied and settled at 330 V, as seen in Fig. 15(a) and (b) while an output voltage is settled at -900V with oscillations and output current is sustained at -90A, as depicted ion Fig. 15(c) and (d).

Case 1: Sag Condition

Fig. 16(a) denotes the power factor waveform with Three Phase AC source current and voltage waveform along with load voltage waveform is depicted in Fig. 16(b)-(d). Here, Power Factor starts with initial deviations before settling down at 1 (unity) which indicates the system undergoes initial power losses which is later stabilized and maintained effectively. Significantly, the second and third graph showcases the Three Phase AC source voltage and current with significant sag, which are maintained between ±400V and ±45A respectively. While, the fourth graph shows both voltage and current in single waveform with the sag condition. Lastly, the fifth graph depicts the load voltage which remains fixed between ±400V throughout the entire time period of 0.8 seconds.

The load voltage progressively increases to ±400 V, then remains constant at the particular voltage level, as seen in Fig. 17 (a-b), while, load current waveform shows, current begins with certain fluctuations before being sustained at ±35A in the depicted time duration of 0.8 seconds, as revealed in Fig. 17(c-d). The load current at the beginning shows certain fluctuations before settling down at the range of ±30 A.

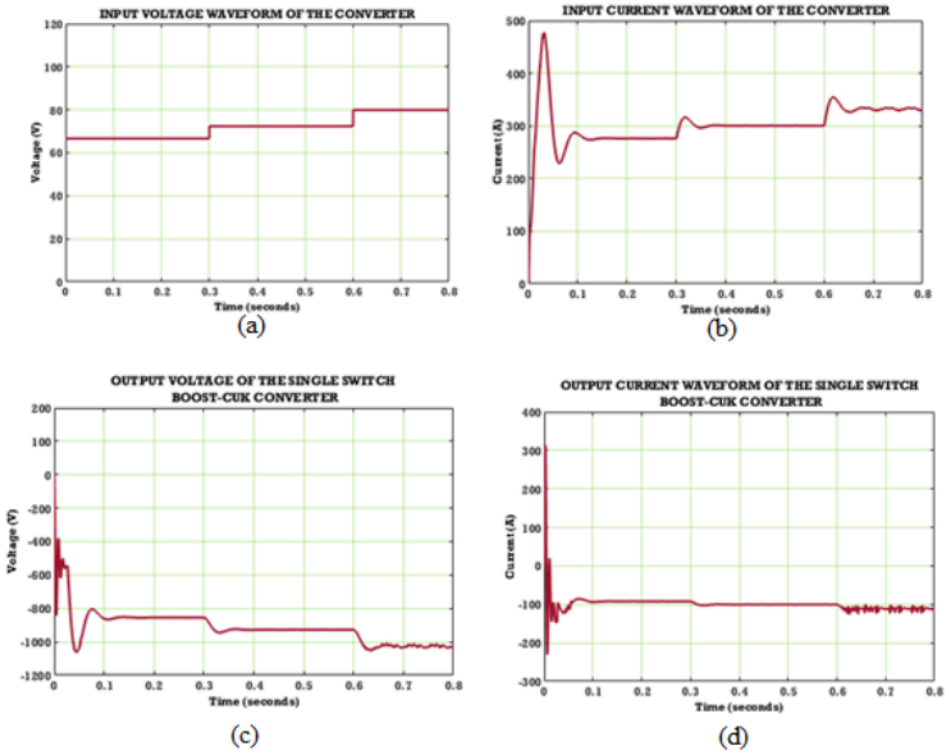

Fig. 15 Converter 's input (a) voltage (b) current and (c) voltage (d) current on output side.

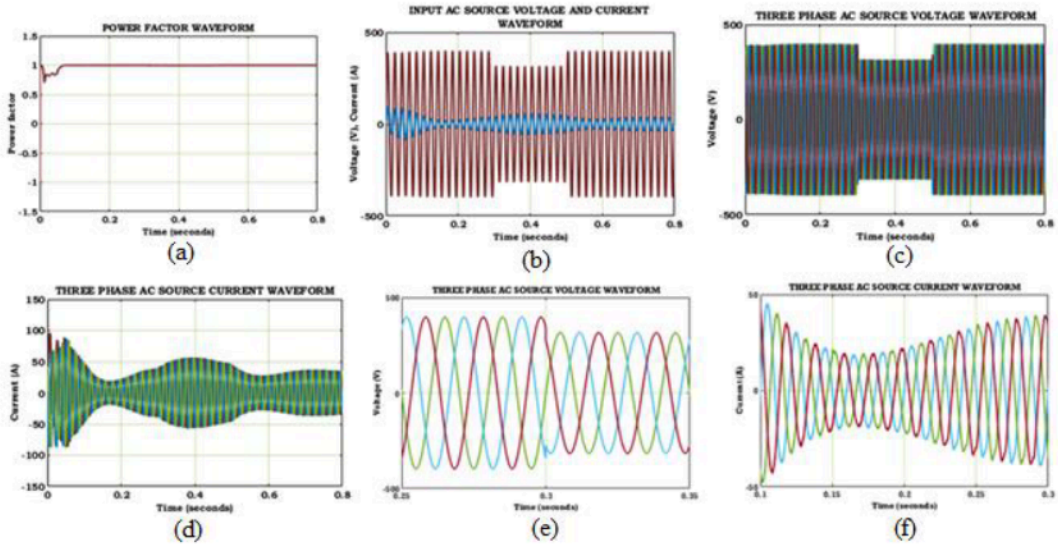

Fig. 16 Waveforms of (a) power factor (b) Ac Source voltage and current (c) source voltage (d) source current (e) zoomed view of voltage (f) current.

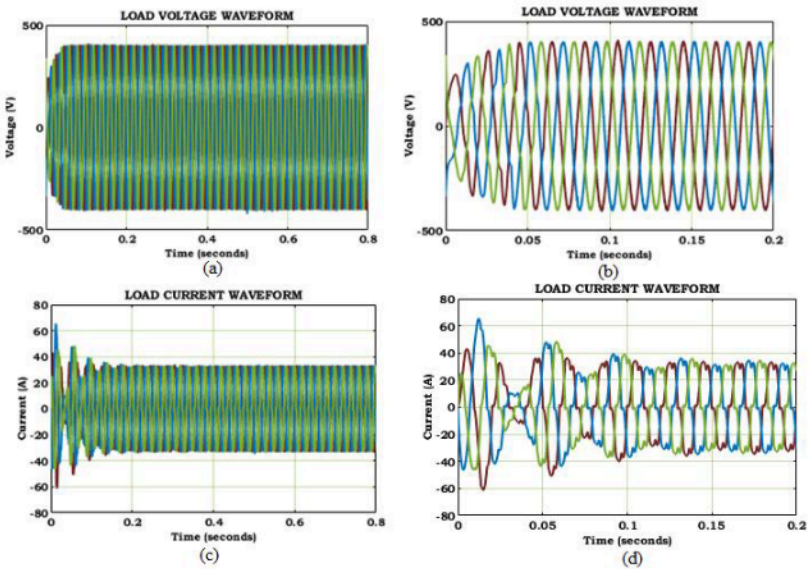

Fig. 17 Load's (a) current (b) voltage waveform and its zoomed view in (c) and (d).

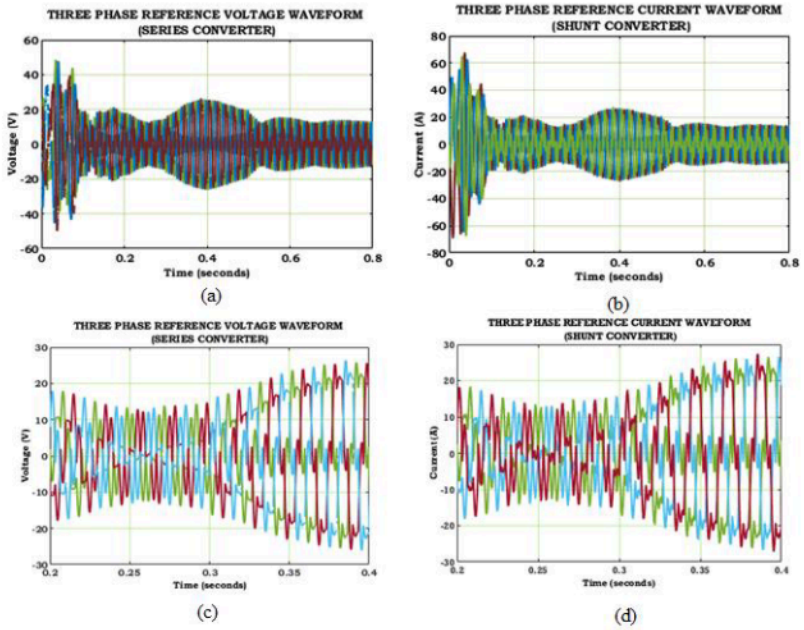

Fig. 18(a) and (c) Reference voltage of series converter and (b) and (d). Reference current of shunt converter.

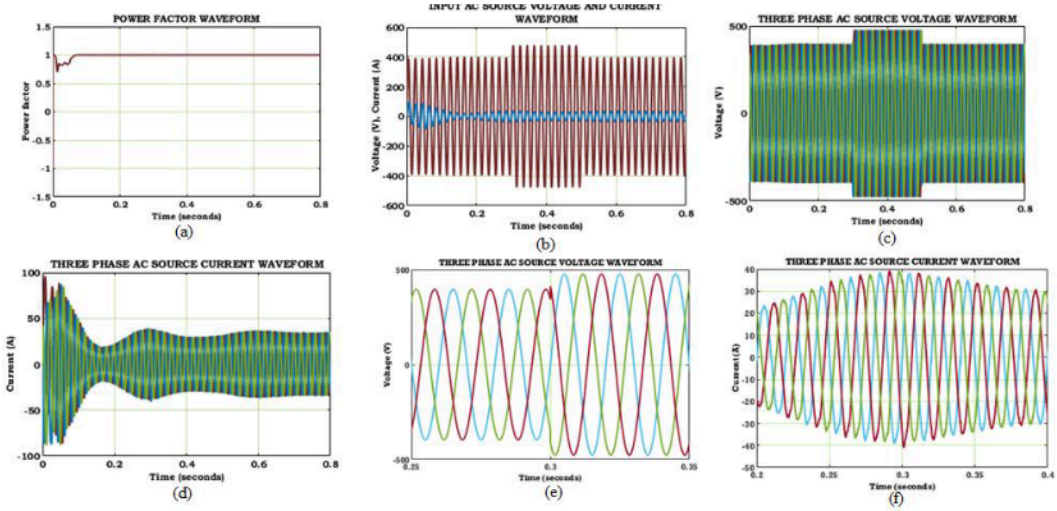

Fig. 19 Waveforms of (a) power factor (b) Ac Source voltage and current (c) source voltage (d) source current (e) zoomed view of voltage (f) current.

Case 2: Swell Condition

Fig. 19(a) showcases the Power factor and load voltage waveform along with the performance of Three Phase AC under swell conditions is shown in Fig. 19(b). The first graph displays the power factor which initially fluctuates, then later stabilizes to 1 (unity). Significantly, the three phase AC source voltage waveform showcases voltage with swell and similarly, the current waveform showcases swell conditions before stabilizing, as seen in Fig. 19(c-f). Both voltage and current waveform along with swell condition, referring to their relationship and variations due to swell.

Fig. 20(a) and (b) denotes the characteristics of load voltage and current. The load voltage gradually increases to ±400 V before stabilizing and the load current initially depicts certain fluctuations which later stabilizes to constant value of ±35 A respectively throughout the given time period of 0.8 seconds.

Fig. 21(a)-(d) displays the Three Phase reference voltage and current waveform, in which the load current exhibits initial fluctuations and then stabilizes around ±30 A. While, both the series converter and the shunt converter showcases certain deviations at the beginning before settling down within the ranges of approximately around ±10 V and ±10 A, respectively.

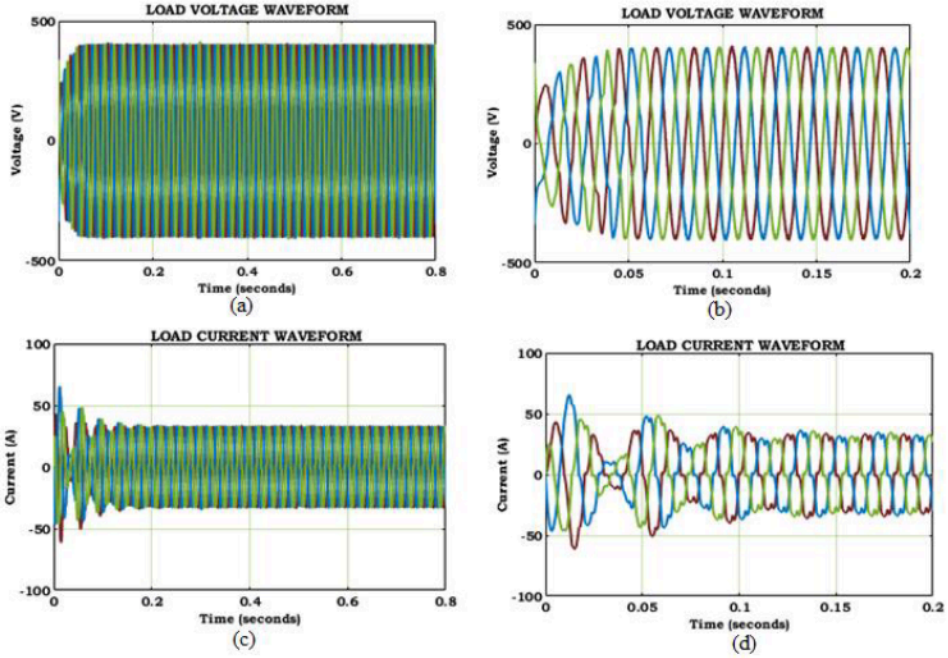

Fig. 20 Load's (a) voltage (b) current waveform and its zoomed view in Fig. 17(c) and (d).

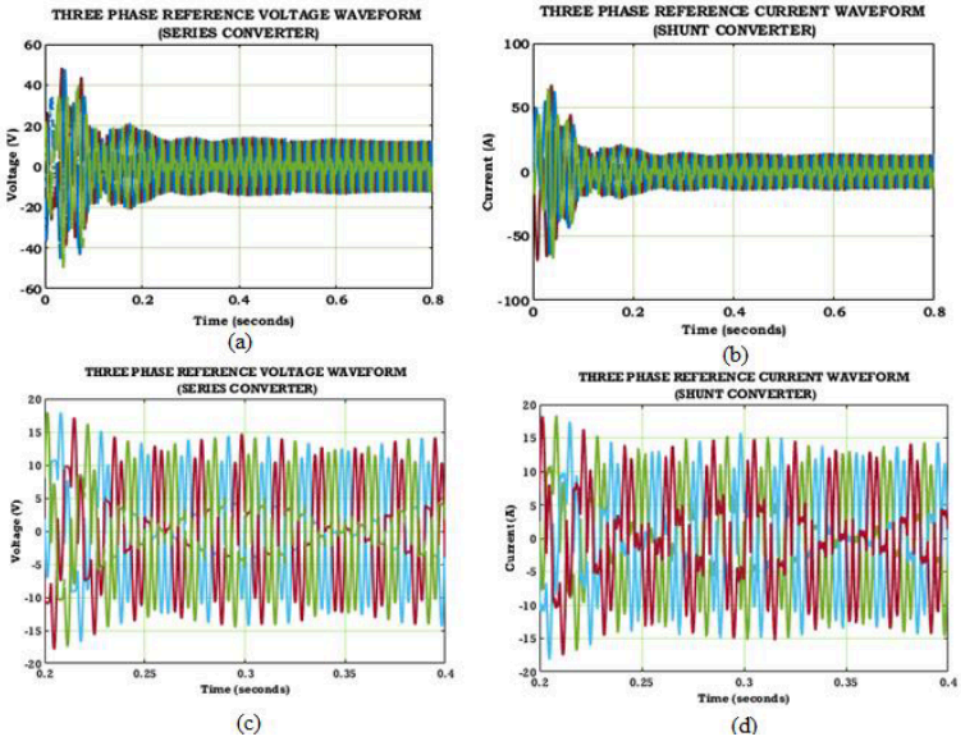

Fig. 21 Three Phase reference waveform for (a) voltage and (b) current (c) Zoomed view of voltage (d) Zoomed view of current.

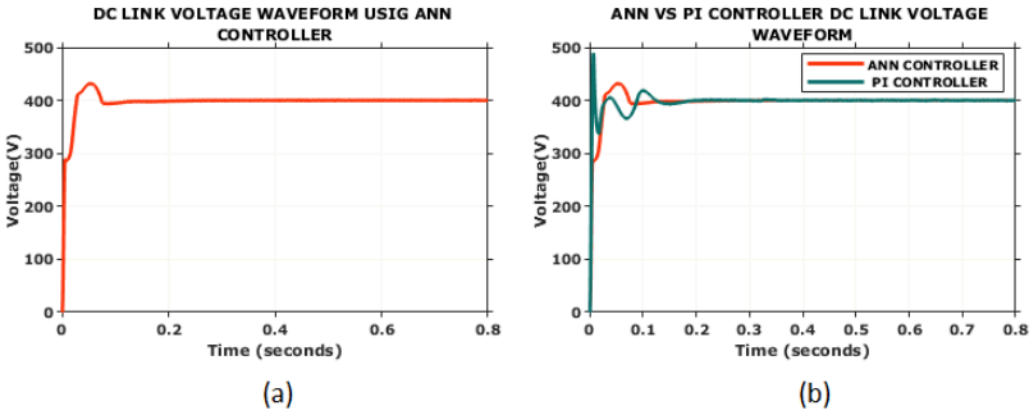

Fig. 22 DC Link voltage (a) ANN controller (b) ANN vs PI controller.

Fig. 22(a) demonstrates that the ANN-based controller outperforms transient response and steady-state accuracy. The suggested ANN regulator successfully adjusts to nonlinear fluctuations in renewable power and load, ensuring a steady DC-link voltage with fewer oscillations and better dynamic stability. Fig.22(b) DC-link voltage (V_{DC}) response comparison of the traditional PI controller and the suggested ANN-based controller.The ANN controller keeps the DC-link voltage to 400 V with little overshoot and faster settling under variable load and renewable input situations.

The performance analysis of PI [27] and ANN controller is depicted in Fig. 23. The ANN controller has the lowest rising and settling time of 0.8 s and 1.5 s, improves the performance of the system.

Fig. 24 represents the comparison of control approaches used for UPFC, like O-FOPID [13] with proposed ANN controller based UPFC. The THD sag and swell attained by ANN-UPFC is comparatively low than O-FOPID. Similarly, the voltage sag and swell compensation attained by ANN-UPFC is higher than O-FOPID, indicating the ANN-UPFC performs better than O-FOPID with enhanced control strategy. The response time required by ANN is quite less, referring to its ability of fast processing. The Power Factor and Efficiency obtained by ANN-UPFC is higher while comparing to O-FOPID, thus, implying that, ANN-UPFC outperforms O-FOPID with improved power quality.

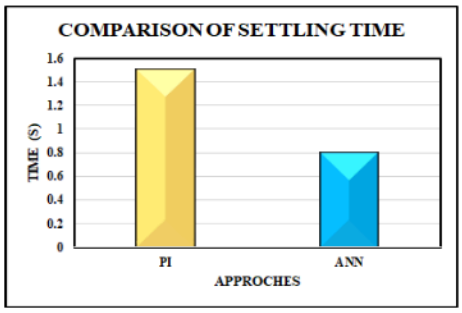

Fig. 23 Comparison of controllers settling time.

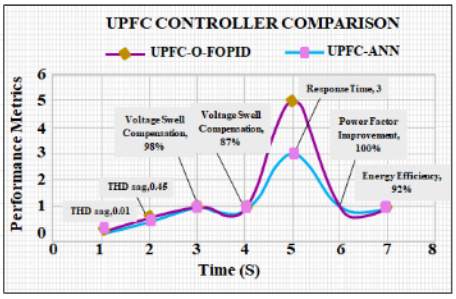

Fig. 24 UPFC Controller comparison.

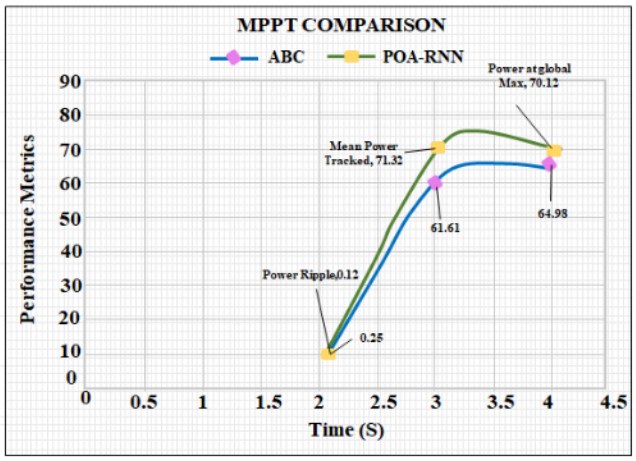

Fig. 25 MPPT performance comparison.

Fig. 25 showcases the performance comparison of proposed POA-RNN based MPPT technique with ABC based MPPT approach [21]. The proposed MPPT approach performs well with reduced, Power Ripple of 0.12 with increased mean power tracked value of 71.32 and power at global maximum being about 70.12, indicating that POA-RNN MPPT attains efficient and reliable tracking with fast convergence and limited fluctuations than that of ABC-MPPT technique.

Fig. 26 demonstrates the tracking efficiency comparison between ABC MPPT, WSO-ANFIS MPPT [26] and POA-RNN MPPT techniques. The proposed MPPT approach attained higher tracking efficiency of 99.8%, implying that POA-RNN MPPT effectively tracks the MPP with increased accuracy surpassing both ABC and WSO-ANFIS MPPT.

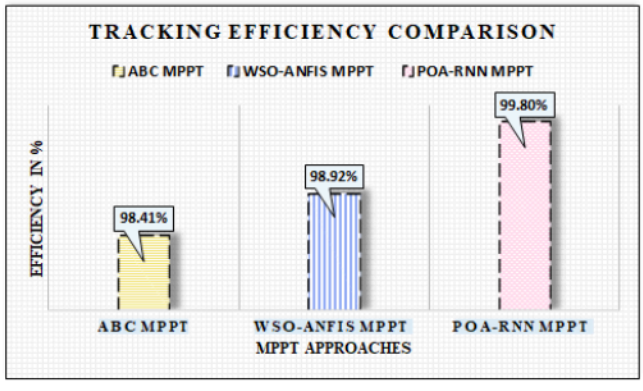

Fig. 26 Comparison of tracking efficiency.

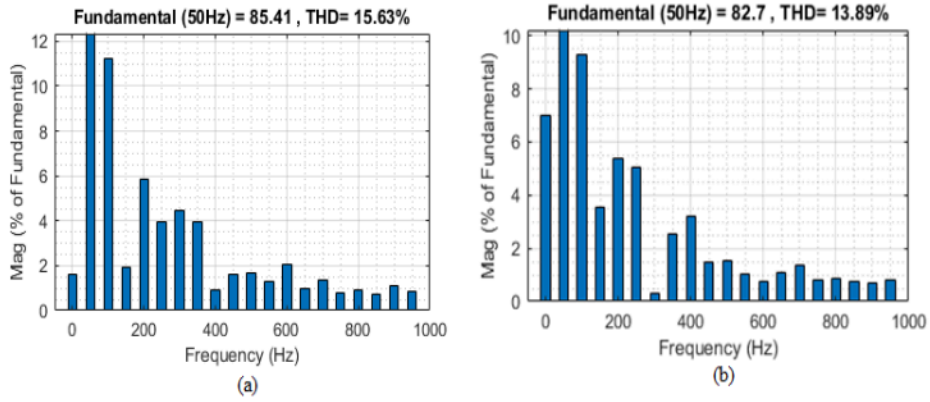

Fig. 27 THD of (a) PI controller (b) FL controller.

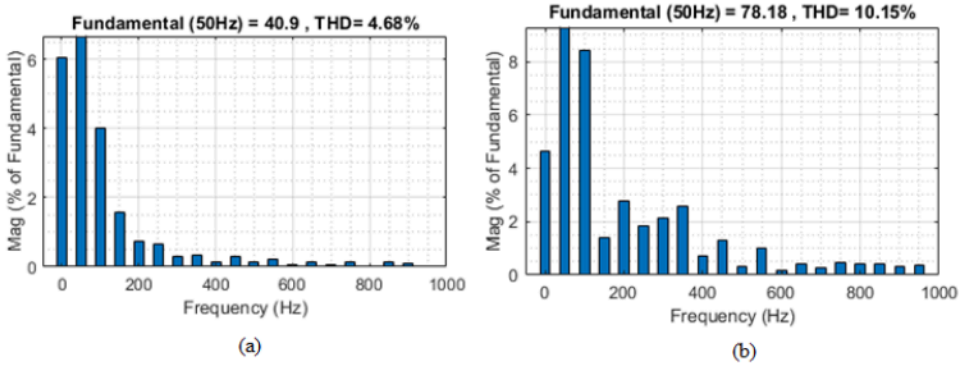

Fig. 28 THD of (a) with ANN controller (b) without ANN controller.

The THD of PI and FLC controller is presented in Fig. 27(a) and (b). The FLC controller has lowest THD of 13.89%. Similarly, the lowest THD is attained by the using ANN controller, is revealed in Fig. 28(a) and 9(b) and table 3.

Table 3 Analysis of THD.

APPRAOCHES	THD (%)
Without ANN	10.15
With ANN	4.68

The outcomes imply that by successfully reducing voltage sag and swell with the ANN-based UPFC controller greatly enhances power quality. Even in the disruption, the system guarantees steady load voltage and current. It improves grid resiliency and dependability while seamlessly incorporating PV power.

4. Conclusion

The proposed system effectively addresses the PQ issues including voltage sag and swell by integrating enhanced control strategies. The deployment of UPFC with an ANN controller increases the system's ability to rectify the PQ issues and achieve optimum power flow. Furthermore, the implementation of PV system using a single switch Boost-Cuk converter assures consistent, reliable and boosted PV power supply to the DC link. Additionally, the deployment of POA-RNN based MPPT ensures maximum power extraction even under varying environmental conditions, thereby improving energy utilization. The validation of the proposed system attained using MATLAB/Simulink showcases that, implemented system depicts improved PQ with reduced power ripple (0.12) and enhanced tracking efficiency (99.8%). Therefore, the developed system assures to address the PQ issues, thus, contributing towards consistent and reliable functioning of power system. Nevertheless, the algorithm's performance is dependent on initial parameter configurations such as population size and iteration counts. In addition, although POA exhibits robust optimization behaviour in simulation, its computational cost could grow with increasing dimension of the problem. These trade-offs will need to be addressed when scaling the system for real-time or hardware-in-the-loop applications.

Author Contributions

Gadupudi Lakshminarayana: Conceptualization, Data Curation, Methodology, Writing – original draft. **Sreedevi Saravanakumar**: Methodology, Project Administration, Validation, Supervision, Writing – review & editing. **Malapati Venkateswarlu**: Methodology, Project Administration, Validation, Supervision, Writing – review & editing. **Thankaraj Retna bai Premila**: Methodology, Project Administration, Validation, Supervision, Writing – review & editing.

Declaration of Interest Statement

The authors declare that they have no known competing financial interests or personal relationships that could have appeared to influence the work reported in this paper.

Reference

[1] Abdelkader, A. B., Mouloudi, Y. and Soumeur, M. A., Integration of renewable energy sources in the dynamic voltage restorer for improving power quality using ANFIS controller. *Journal of King Saud University-Engineering Sciences.* 35 (2023) 539–548, doi: https://doi.org/10.1016/j.jksues.2022.11.002.

[2] Viswanatha Rao, J. and Lakshminarayana, G. Estimation and Moderation of Harmonics in Distribution Systems. In *International Conference on Intelligent Manufacturing and Energy Sustainability (ICIMES-2019)*. (2020), 353-360, doi: https://doi.org/10.1007/978-981-15-1616-0_34.

[3] Madhusudhanan, J. and Santhosh Kumar, G., 9-Level VSC based STATCOM for reactive power management and voltage stability improvement. *Journal of Green Engineering*. 10 (2020) 10275–10288.

[4] Rajput, M. S. and Namdeo, A. K., Optimizing control of UPFC AI based dual converter technology for grid integrated PV system. *Journal of Computing Technologies (JCT).* 12 (2023) 1-7.

[5] Jayatheertha, H. J., Smart method for minimising transmission line losses. *International Journal of Control Theory and Applications*. 9 (2016) 175–181.

[6] Valuva, C. and Chinnamuthu, S., Performance analysis of marine-predator-algorithm-based optimum PI controller with unified power flow controller for loss reduction in wind–solar integrated system. *Energies*. 16 (2023) 6157, doi: https://doi.org/10.3390/en16176157.

[7] Iqbal, A., Waqar, A., Elavarasan, R. M., Premkumar, M., Ahmed, T., Subramaniam, U. and Mekhilef, S., Stability assessment and performance analysis of new controller for power quality conditioning in microgrids. *International Transactions on Electrical Energy Systems*. 31 (2021) e12891, doi: https://doi.org/10.1002/2050-7038.12891.

[8] Goud, B. S., Reddy, C. R., Bajaj, M., Elattar, E. E. and Kamel, S., Power quality improvement using distributed power flow controller with BWO-based FOPID controller. *Sustainability*. 13 (2021) 11194, doi: https://doi.org/10.3390/su132011194.

[9] Dheeban, S. S. and Muthu Selvan, N. B., ANFIS-based power quality improvement by photovoltaic integrated UPQC at distribution system. *IETE Journal of Research*. 69 (2023) 2353–2371, doi: https://doi.org/10.1080/03772063.2021.1888325.

[10] Gadupudi, L., Rao, G. S., Divakar, R. V. L. N., Malik, H., Alsaif, F., Alsulamy, S. and Ustun, T. S., Fuzzy-based fifteen-level VSC for STATCOM operations with single DC-Link voltage. *Sustainability*. 15 (2023) 6188, doi: https://doi.org/10.3390/su15076188.

[11] Gadupudi, M.L. and Rao, G.S., 7-Level Transformers Integrated Voltage Source Converter Based STATCOM for Voltage Profile Enhancement. *Solid State Technology*. 63 (2020) 3134-3141.

[12] Prasad, D. and Dhanamjayulu, C., Solar PV-fed multilevel inverter with series compensator for power quality improvement in grid-connected systems. *IEEE Access*. 10 (2022) 81203–81219, doi: https://doi.org/10.1109/ACCESS.2022.3196174.

[13] Thumu, R., Reddy, K. H. and Reddy, C. R., Unified power flow controller in grid-connected hybrid renewable energy system for power flow control using an elitist control strategy. *Transactions of the Institute of Measurement and Control*. 43(2020) 228–247, doi: https://doi.org/10.1177/0142331220957890.

[14] Illa, V. R., Senapati, R. U. and Swain, S. C., Implementation of UPQC alleviating power quality issues in a hybrid grid integrated system. *WSEAS Transactions on Power Systems.* 16 (2021) 316–335, doi: https://doi.org/10.37394/232016.2021.16.32.

[15] Ravi, T., Kumar, K. S., Dhanamjayulu, C., Khan, B. and Rajalakshmi, K., Analysis and mitigation of PQ disturbances in grid connected system using fuzzy logic based IUPQC. *Scientific Reports*. 13 (2023) 22425, doi: https://doi.org/10.1038/s41598-023-49042-z.

[16] Yadav, S. K., Patel, A. and Mathur, H. D., PSO-based online PI tuning of UPQC-DG in real-time. *IEEE Open Journal of Power Electronics*. 5 (2024)1419-1431, doi: https://doi.org/10.1109/OJPEL.2024.3445719.

[17] Murugan, S. and Ashly Beby, M. L., Improvement of unified power quality conditioner based on GA optimized NN controller. *International Journal of Electrical Engineering*. 7 (2014) 25–34.

[18] Venkatesan, R., Kumar, C., Balamurugan, C. R. and Senjyu, T., Enhancing power quality in grid-connected hybrid renewable energy systems using UPQC and optimized O-FOPID, *Frontiers in Energy Research*. 12 (2024) 1425412, doi: https://doi.org/10.3389/fenrg.2024.1425412.

[19] Reddy, C. R., Goud, B. S., Aymen, F., Rao, G. S. and Bortoni, E. C., Power quality improvement in HRES grid connected system with FOPID based atom search optimization technique. *Energies*. 14 (2021) 5812, doi: https://doi.org/10.3390/en14185812.

[20] Kavin, K. S., Karuvelam, P. S., Raj, M. D. and Sivasubramanian, M., A novel KSK converter with machine learning MPPT for PV applications. *Electric Power Components and Systems.*(2024) 1-19, doi: https://doi.org/10.1080/15325008.2024.2346806.

[21] Gadupudi, L. N., Rao, G. S., Devarapalli, R. and García Márquez, F. P., Seven level voltage source converter based static synchronous compensator with a constant DC-Link voltage. *Applied Sciences*. 11 (2021) 7330, doi: https://doi.org/10.3390/app11167330.

[22] Darwish, A., A bidirectional modular Cuk-based power converter for shore power renewable energy systems. *Energies*. 16 (2022) 274, doi: https://doi.org/10.3390/en16010274.

[23] Mittal, M. B. and Yadav, D. L., Hybrid energy management and control strategy through UPFC with PID and FLC. *International Journal of Artificial Intelligence and Mechatronics.*11 (2023) 97–119.

[24] González-Castaño, C., Restrepo, C., Kouro, S. and Rodriguez, J., MPPT algorithm based on artificial bee colony for PV system. *IEEE Access.* 9 (2021) 43121–43133, doi: https://doi.org/10.1109/ACCESS.2021.3066281.

[25] Ali, A. I. M., Mousa, H. H., Mohamed, H. R., Kamel, S., Hassan, A. S., Alaas, Z. M., Mohamed, E. E. and Abdallah, A. R., An enhanced P&O MPPT algorithm with concise search area for grid-tied PV systems. *IEEE Access*. 11 (2023) 79408–79421, doi: https://doi.org/10.1109/ACCESS.2023.3298106.

[26] Sathyapriya, R. and Jayalakshmi, V., HRES integrated DSTATCOM using high gain Sepic-Zeta based WOA optimized ANFIS-MPPT controller for PQ issues. *Journal of Electrical Systems*. 20 (2024) 149–164, doi: https://doi.org/10.52783/jes.1118.

[27] Himabindu, E., Krishna, D., Venkateshwarlu, S. and Reddy, K. C., Fuzzy Logic Sliding Mode Controller based UPQC using DC Link Voltage fed by solar PV to enhance dynamic performance in the power grid. *Journal of Applied Science and Engineering*. 28 (2024) 969–978, doi: https://doi.org/10.6180/jase.202505_28 (5).0006.